View metadata, citation and similar papers at core.ac.uk
brought to you by CORE
provided by Institutional Repository of the Freie Universität Berlin

Quantum paramagnet in a π flux triangular lattice Hubbard model

Stephan Rachel,[1] Manuel Laubach,[2] Johannes Reuther,[3,4] and Ronny Thomale[2]

[1] *Institute for Theoretical Physics, Technische Universität Dresden, 01062 Dresden, Germany*
[2] *Institute for Theoretical Physics, University of Würzburg, 97074 Würzburg, Germany*
[3] *Dahlem Center for Complex Quantum Systems and Fachbereich Physik, Freie Universität Berlin, 14195 Berlin, Germany*
[4] *Helmholtz-Zentrum Berlin für Materialien und Energie, 14109 Berlin, Germany*

(Dated: April 8, 2015)

We propose the π flux triangular lattice Hubbard model (π-THM) as a prototypical setup to stabilize magnetically disordered quantum states of matter in the presence of charge fluctuations. The quantum paramagnetic domain of the π-THM which we identify for intermediate Hubbard U is framed by a Dirac semi-metal for weak coupling and by 120° Néel order for strong coupling. Generalizing the Klein duality from spin Hamiltonians to tight-binding models, the π-THM maps to a Hubbard model which corresponds to the $(J_{\rm H}, J_{\rm K}) = (-1, 2)$ Heisenberg-Kitaev model in its strong coupling limit. The π-THM provides a promising microscopic testing ground for exotic finite-U spin liquid ground states amenable to numerical investigation.

PACS numbers: 75.10.Kt,71.10.Fd,71.10.Hf

arXiv:1411.4649v2 [cond-mat.str-el] 7 Apr 2015

Introduction. Two-dimensional quantum paramagnets such as spin liquids or valence bond crystals are quantum states of matter that, albeit their enormous diversity from a theoretical standpoint, are hard to find in experimental scenarios [1–4]. At the level of theoretical identification in microscopic models, recent numerical advances such as two-dimensional density matrix renormalization group [5–7], pseudofermion renormalization group [8], or variational Monte Carlo [9, 10] could provide substantiated support for spin liquid regimes. Predominantly, the strong coupling limit of a Mott state is considered which is parametrized by spin exchange interactions.

An exception constitutes the work by Meng *et al.* on the Hubbard model for the honeycomb lattice, where quantum Monte Carlo algorithms avoid the sign problem due to lattice bipartiteness [11]. Small system sizes suggested a non-magnetic insulating regime without valence bond crystal order [11]. As larger scale calculations [12] and more refined determinations of the order parameter [13, 14] revealed, however, the metal insulator transition turns out to be of Gross-Neveu type, where antiferromagnetic order sets in immediately. This is confirmed by cluster methods operating at intermediate Hubbard U [15, 16]. What can still be taken as a motivation from this finding is that a Dirac metal for weak coupling might contribute to a promising scenario for an unconventional metal-insulator transition and exotic phases at intermediate coupling, which is the starting point of our analysis.

In this Letter, we propose the Hubbard model on the π flux triangular lattice (π-THM) as a prototypical candidate for quantum paramagnetic phases at intermediate coupling. In its weak coupling limit, the band structure of the π-THM is semi-metallic, exhibiting the same low-energy behavior as graphene with a different Fermi velocity. The stability of this semi-metal with respect to weak local Coulomb interactions follows from generic properties of Dirac electrons [17, 18]. In its strong-coupling limit, positive and negative hoppings give rise to the same spin exchange amplitude $J = 4(\pm t)^2/U$, rendering the π-THM identical to the nearest-neighbor Heisenberg model on the triangular lattice yielding 120° Néel order [19]. Generalizing the Klein duality [20–23] from spin models to tight-binding models, we can relate the π-THM to a transformed Hubbard model with bond-selective Kitaev-like hopping amplitudes. The strong coupling limit of this Klein-transformed model is given by the $(J_{\rm H}, J_{\rm K}) = (-1, 2)$ Heisenberg-Kitaev model.

As the weak and strong coupling limits are fixed, it remains to be investigated whether there is a direct semi-metal to magnet transition, or whether an intermediate paramagnetic domain emerges at the metal insulator transition. We will explicate below that perturbing away from its infinite-U limit, the short-range resonating valence bond (RVB) loops lower the energy in the π-THM more significantly than for the regular Hubbard model on the triangular lattice (THM). These perturbative arguments are supplemented by the calculation of single-particle spectral functions and ordering tendencies via variational cluster approximation (VCA). For intermediate Hubbard U, we find an extended non-magnetic insulating regime, which promises to host unconventional quantum paramagnetic states of matter.

π-THM. We consider a triangular lattice with an alternating flux pattern such that a triangle threaded by a π flux is surrounded by three triangles which are flux-free (Fig. 1a). Note that triggered by the success in formulating and manufacturing flux lattices through artificial gauge fields in ultra-cold atomic gases [24–26], flux patterns in lattice models have become an experimentally relevant topic in contemporary AMO physics. Of particular importance is the recent proposal of "shaking" an

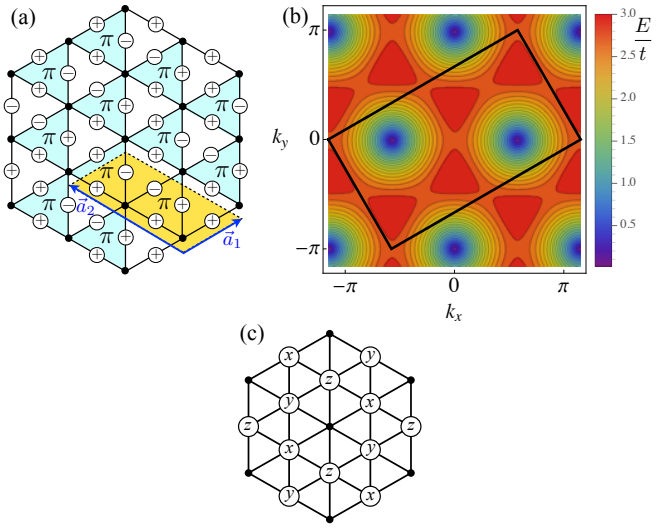

FIG. 1. (Color online) a) Flux pattern and signs of the real nearest neighbor hoppings on the triangular lattice. The π's denote triangles which are threaded by a π flux. b) Contour plot of the spin-degenerate upper band of the semi-metallic band structure (blue spots indicate the Dirac nodes at zero energy); the lower band follows from particle-hole symmetry. The Brillouin zone (black) is spanned by the reciprocal vectors $\boldsymbol{b}_1 = \frac{2\pi}{\sqrt{3}}(1,\sqrt{3})$ and $\boldsymbol{b}_2 = \frac{2\pi}{\sqrt{3}}(-1/2,\sqrt{3}/2)$. (c) four-sublattice structure of a Klein transformation. "x", "y" and "z" indicate the axis around which a spin rotation of angle π is performed. The full dot sublattice remains unchanged.

optical lattice, *i.e.*, to apply a periodic force pulse to the optical lattice. It has been shown that staggered flux patterns for triangular lattices can be achieved [27]. As the Hubbard coupling can be naturally adjusted by the optical setup, this might be one promising route towards realizing the model subject to this paper.

In Fig. 1a, the signs of the real nearest-neighbor hoppings t_{ij} are shown which reproduce the alternating flux pattern; the two-atomic unit cell is shown in yellow spanned by the primitive vectors $\boldsymbol{a}_1 = (\sqrt{3}/2, 1/2)$ and $\boldsymbol{a}_2 = (-\sqrt{3}, 1)$. (We set the lattice spacing $a \equiv 1$ throughout the paper.) The band structure is spin-degenerate and particle-hole symmetric. The Bloch matrix reads $h(\boldsymbol{k}) = \sum_{\boldsymbol{k}} \boldsymbol{d}(\boldsymbol{k}) \cdot \boldsymbol{\sigma}$, where σ^α are Pauli matrices related to the sublattice degree of freedom and

$$\boldsymbol{d}(\boldsymbol{k}) = t \begin{pmatrix} 1 + \cos \boldsymbol{a}_1\boldsymbol{k} + \cos \boldsymbol{a}_2\boldsymbol{k} - \cos(\boldsymbol{a}_1 + \boldsymbol{a}_2)\boldsymbol{k} \\ \sin \boldsymbol{a}_1\boldsymbol{k} - \sin \boldsymbol{a}_2\boldsymbol{k} + \sin(\boldsymbol{a}_1 + \boldsymbol{a}_2)\boldsymbol{k} \\ 2\cos \boldsymbol{a}_1\boldsymbol{k} \end{pmatrix}. \tag{1}$$

We find the single particle spectrum $\varepsilon_\sigma^\pm = \pm\sqrt{d^2}$ which is shown as a contour plot in Fig. 1b. The Dirac nodes are located at $K^\pm = (\pm\pi/\sqrt{3}, 0)$. Expanding around the Dirac nodes yields the Lorentz-invariant Dirac theory of graphene, along with valley and spin degeneracy and a bare Fermi-velocity $v_F = \sqrt{6}t$. Note that this type of band structure has been previously mentioned as a mean field spectrum of a U(1) liquid candidate (dubbed U1B) [28]. Adding Hubbard interactions, we find the π-THM governed by the Hamiltonian

$$\mathcal{H}_{\pi\text{-THM}} = \sum_{\langle ij\rangle,\sigma} \left(t_{ij} c_{i\sigma}^\dagger c_{j\sigma} + \text{h.c.} \right) + U \sum_i n_{i\uparrow} n_{i\downarrow}, \tag{2}$$

where $n_{i\sigma} = c_{i\sigma}^\dagger c_{i\sigma}$ denotes the density operator of electrons at site i with spin σ.

Klein-duality map from a Kitaev-Hubbard model. The π flux pattern on the triangular lattice allows to draw subtle connections to iridium-based transition metal oxides and Heisenberg-Kitaev models [21]. Originally proposed for the honeycomb iridates $(\text{Na,Li})_2\text{IrO}_3$ [21], the Heisenberg-Kitaev model reads

$$\mathcal{H}_{\text{HK}} = \sum_{\langle ij\rangle} J_{\text{H}} \boldsymbol{S}_i \boldsymbol{S}_j + J_{\text{K}} S_i^\gamma S_j^\gamma, \tag{3}$$

where, for the triangular lattice, we define $\gamma = x$ for bonds along the $\boldsymbol{a}_1$ direction, $\gamma = y$ along the $\boldsymbol{a}_2$ direction, and $\gamma = z$ along the vertical bonds.

We define the class of Kitaev-Hubbard models as tight-binding band structures subject to local Hubbard U which, in the limit of infinite U, map onto a Heisenberg-Kitaev model (3). As explicated below, we can formulate a Klein duality map from our π-THM to such a Kitaev-Hubbard model. In the past, Klein dualities have been successfully applied to spin Hamiltonians [20–23]. Here, we generalize the Klein duality to Hubbard models, *i.e.*, to creation and annihilation operators of electrons. As for the spin models, we define four sublattices on the triangular lattice as shown in Fig. 1c, and then rotate the spin of the creation/annihilation operators on the different sublattices: we rotate the first sublattice around the x axis by π, the second around the y axis by π, the third around the z axis by π, and the fourth sublattice remains unchanged (Fig. 1c). Such spin rotations are easily accomplished by virtue of Pauli matrices, $\mathcal{U}_\alpha = \exp(i\frac{\pi}{2}\sigma^\alpha) = i\sigma^\alpha$ and $\mathcal{U}^{\alpha\,\dagger} = -i\sigma^\alpha$ for rotations around the α axis ($\alpha = x, y, z$). The Klein-transformed version of Eq. (2) is given by a Kitaev-Hubbard model with a kinetic term $H_0 = it\sum_{\langle ij\rangle} \nu_{ij} c_{i\alpha}^\dagger \sigma_{\alpha\beta}^\gamma c_{j\beta}$ where $\gamma = x, y, z$ are defined as in (3), and σ^γ denote Pauli matrices describing the spin degrees of freedom. The phase convention $\nu_{ij} = \pm 1$ is chosen such that the hopping amplitude is positive in $\boldsymbol{a}_1$, $\boldsymbol{a}_2$ and $(2\boldsymbol{a}_1 + \boldsymbol{a}_2)$ directions and negative in opposite directions. The Hubbard term $U n_{i\uparrow} n_{i\downarrow}$ is invariant under the Klein map. In the strong coupling limit, this Kitaev-Hubbard model becomes the $(J_{\text{H}}, J_{\text{K}}) = (-1, 2)$ Kitaev-Heisenberg model of Eq. (3).

Depending on the specific values of J_{H} and J_{K}, the model in Eq. (3) might give rise to nonmagnetic phases of triangular layered iridate compounds [29–31]. From the classical analysis, the $(J_{\text{H}}, J_{\text{K}}) = (-1, 2)$ point in

Eq. (3) is surrounded by a $\mathbb{Z}_2$ vortex lattice [32]. As such, the Klein map suggests that charge fluctuations in the π-THM, as implied by finite U, may trigger similarly interesting effects as for the vortex lattice.

Variational Cluster Approximation. VCA is a quantum cluster approach to compute single-particle spectral functions for interacting many-body systems [33]. One first solves a small cluster (with typically four to twelve lattice sites) exactly and derives the corresponding full Green's function. Using the framework of self-energy functional theory [34], one obtains the full Green's function of an infinitely large lattice which is covered by the clusters, and the individual clusters are coupled by hopping terms only. The latter step represents a significant approximation to the full many-body problem, while the method still includes spatial quantum correlations. Embedded into a grand-canonical ensemble, the configuration with lowest energy is found by varying the chemical potential as well as all single-particle parameters which may also include the bare hopping amplitudes [16]. Three comments about the VCA are in order which are important for the analysis of our π-THM. (i) Variation of the hopping t is crucial in order to guarantee the stability of the semi-metal with respect to small U. (ii) Using the same setup and accuracy which due to (i) exceeds most previous VCA calculations, we do not find a nonmagnetic insulator (NMI) phase within the honeycomb lattice Hubbard model for intermediate U [16] as a benchmark. (iii) The magnetic instability is investigated by means of Weiss fields. For the 120° Néel order, only clusters with multiples of three lattice sites can be used. In conjunction with the two-atomic unit cell, only 6 and 12 site clusters are in principle suitable for the analysis of the π-THM. Preference is of course given to 12, *i.e.*, the largest available cluster.

Phase diagram. For the quantitative analysis, we employ a super-cluster construction with a 12-site and mirror-12-site cluster (see inset Fig. 2) We first pin the Dirac metal-insulator transition by determining the opening of the charge gap Δ_c at $U/t = 9.5$ (blue domain in Fig. 2). Note that this happens at comparably large U, in accordance with the small spectral weight of the Dirac metal nearby the Fermi level. In the infinite coupling limit, the nearest neighbor Heisenberg term $J = 4t^2/U$ dominates the virtual spatial fluctuation processes. We apply the Weiss field associated with 120° Néel order and determine the response of the π-THM. We find magnetic order ranging only down to $U/t = 13.4$ (red domain in Fig. 2). This finding is remarkable, as the regular THM, investigated for the same setting, allows for magnetic ordering to the lower value of $U/t = 8.5$. (Quantitative deviations from previous VCA investigations of the regular THM [35] derive from our consideration of cluster hopping variation.) This can be understood from a strong coupling expansion [36]. For the π-THM, up to order

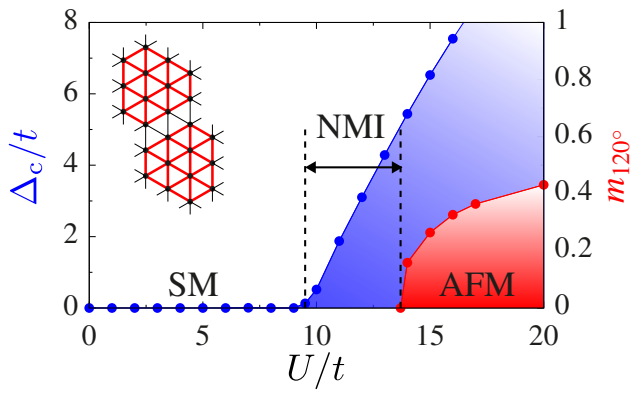

FIG. 2. (Color online). Phase diagram of (2) as obtained by VCA. U_{c1}, U_{c2}, Δ_c, and m_{120° are calculated for a lattice covering with 12-site (mirror) clusters as sketched in the inset (the magnetization $m_{120^\circ} = 1$ denotes the saturation value). From single-particle spectra, there are three phases: semimetal (SM), non-magnetic insulator (NMI), and 120° Néel antiferromagnetic insulator (AFM).

t^4/U^3, we find

$$\mathcal{H}^{(4)}_{\pi\text{-THM}} = \left(\frac{4t^2}{U} + \frac{12t^4}{U^3}\right)\sum_{\langle ij\rangle} \boldsymbol{S}_i\boldsymbol{S}_j + \frac{12t^4}{U^3}\sum_{\langle\langle ij\rangle\rangle} \boldsymbol{S}_i\boldsymbol{S}_j + \frac{4t^4}{U^3}\sum_{\langle\langle\langle ij\rangle\rangle\rangle} \boldsymbol{S}_i\boldsymbol{S}_j - \frac{80t^4}{U^3}\sum_p \Big[(\boldsymbol{S}_1\boldsymbol{S}_2)(\boldsymbol{S}_3\boldsymbol{S}_4) + (\boldsymbol{S}_2\boldsymbol{S}_3)(\boldsymbol{S}_1\boldsymbol{S}_4) - (\boldsymbol{S}_1\boldsymbol{S}_3)(\boldsymbol{S}_2\boldsymbol{S}_4)\Big] , \quad (4)$$

where we use the standard notations $\langle ij\rangle$, $\langle\langle ij\rangle\rangle$, and $\langle\langle\langle ij\rangle\rangle\rangle$ for first, second, and third nearest neighbors, and $\sum_p$ indicates the summation over all parallelograms (including different orientations) which consist of two triangles, $\triangle\triangledown$, where the long diagonal on the parallelogram is a link between the sites with indices "2" and "4". (Note that spin Hamiltonians including a ring exchange term such as (4) were studied previously on the triangular lattice, albeit for arbitrary coefficients independent of a strong coupling expansion. There, a limited range on the Heisenberg exchange coupling was assumed, constraining it up to second [37] or nearest neigbor [38].) Comparing π-THM against the regular THM [39, 40], one difference is the reversed sign for the plaquette term coefficient in (4). We compute the strength of dimer resonances to investigate the effect of such higher order contributions. Given a dimer loop, the transition matrix element $|E_{12}|$ between two dimer configurations on that loop determines the energy gain associated with such a resonance. For a loop on a 2×2 plaquette, this reads

$$E_{12} = \langle \; \square \; | \mathcal{H}^{(4)}_{\pi\text{-THM}} | \; \square \; \rangle \; , \quad (5)$$

where

$$| \; {}^{1}_{2}\square^{4}_{3} \; \rangle = \frac{1}{2}(|\uparrow_1\downarrow_2\rangle - |\downarrow_1\uparrow_2\rangle)(|\uparrow_3\downarrow_4\rangle - |\downarrow_3\uparrow_4\rangle) \; . \quad (6)$$

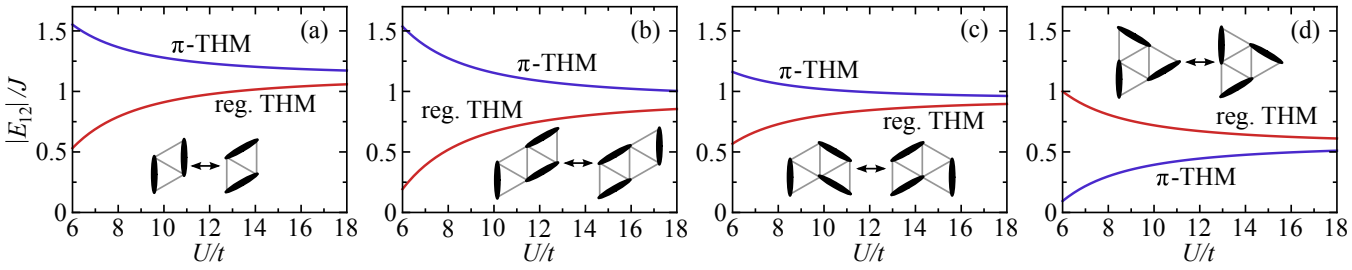

FIG. 3. (Color online). Strength of dimer loop resonances $|E_{12}|$ (see Eqs. 5 and 6) for the 4-site loop in panel (a) and all 6-site loops in panels (b) - (d) calculated for the π-THM and the regular THM. The insets illustrate the according resonances. Except for (d), dimer resonances result in a larger energy gain for the π-THM than the regular THM.

In Eq. 5 the Hamiltonian $\mathcal{H}^{(4)}_{\pi\text{-THM}}$ is restricted to a 2×2 plaquette. Resonances for longer dimer loops may be calculated similarly. In Fig. 3, we show the energy gain $|E_{12}|$ for resonances on all dimer loops with a length of 4 and 6 lattice spacings. For the shortest 4-site loop (Fig. 3a), $|E_{12}|$ is larger for the π-THM than for the regular THM. This picture diversifies as we consider longer-loop contributions (Figs. 3(b)-(d)), while the general trend from the smallest loop size persists. The enhanced dimer resonances give a natural explanation for the quick drop of magnetic order in the π-THM upon decreasing U/t. Whether a valence bond crystal, i.e. the onset of translational symmetry breaking, or a spin liquid state might be preferred cannot be inferred from this consideration. (At least note that the dimer resonance does not significantly drop from a 2-site loop to 6-site loops, which might suggest a possibly sizable resonance to long-range dimer loops along the RVB liquid paradigm [41–43]; see also Refs. [44, 45].) Similarly, our analysis does not allow to determine whether the non-magnetic insulating domain (Fig. 2) is composed out of one or several distinct paramagnetic phases. What our VCA analysis does allow to determine, however, is whether collinear magnetic order can be stabilized, as a recent variational Monte Carlo study [37] of a similar model as Eq. (4) suggests: in the parameter range $5 < U/t < 15$, we cannot find a stationary point for the collinear magnet, thus rejecting it as a candidate ground state. Another direction to further understand the NMI phase within VCA might be to allow for spatially anisotropic hoppings, where a similarly big NMI domain has been found previously (see *e.g.* Ref. [46]).

Conclusion. We have proposed the Hubbard model on the π flux triangular lattice to consitute a paradigmatic scenario for quantum paramagnets at intermediate coupling. Via VCA, we find a non-magnetic insulating regime for $9.5 < U/t < 13.4$ framed by a Dirac semimetal and 120° Néel order which only establishes itself close to the strong coupling limit because of significant quantum fluctuations. The dimer resonances of the π-THM provide further support for its propensity towards quantum paramagnetic phases.

Several directions might be interesting to follow up on this work. First, additional methodological approaches should be applied to further resolve the nature of the paramagnetic domain in the π-THM. Second, it is worth investigating possible experimental realizations in the context of ultra-cold atomic fermionic gases deposited in optical flux lattices. In addition, the Klein-transformed Hubbard model derived from the π-THM might be applicable to the iridate triangular compounds where a joint perspective from Heisenberg-Kitaev models and charge fluctuations due to finite Hubbard U might be indispensable. Third, from a broader perspective, the Klein duality mapping of Hubbard models can establish a valuable new tool to derive interesting connections between different lattice Hamiltonians, where one model allows to draw implications on the other.

We thank F. F. Assaad, L. Balents, S. Bieri, M. Vojta, and S. Wessel for discussions. We are grateful to O. Motrunich for pointing out to us Ref. [28]. SR is supported by DFG-FOR 960, DFG-SPP 1666, DFG-SFB 1143, and by the Helmholtz association through VI-521. JR acknowledges support from the Deutsche Akademie der Naturforscher Leopoldina through grant LPDS 2011-14. ML and RT are supported by the ERC starting grant TOPOLECTRICS (ERC-StG-Thomale-336012) and by the National Science Foundation under Grant No. NSF PHY11-25915. We thank the Center for Information Services and High Performance Computing (ZIH) at TU Dresden for generous allocations of computer time.

[1] *Frustrated spin systems*, edited by H. T. Diep (World Scientific, Singapore, 2004).
[2] C. Lacroix, P. Mendels, and F. Mila, *Introduction to Frustrated Magnetism: Materials, Experiments, Theory* (Springer, Berlin, 2011), Vol. 164.
[3] P. A. Lee, Science **321**, 1306 (2008).
[4] L. Balents, Nature **464**, 199 (2010).
[5] S. Yan, D. A. Huse, and S. R. White, Science **332**, 1173 (2011).
[6] H.-C. Jiang, H. Yao, and L. Balents, Phys. Rev. B **86**, 024424 (2012).

[7] S. Depenbrock, I. P. McCulloch, and U. Schollwöck, Phys. Rev. Lett. **109**, 067201 (2012).
[8] R. Suttner, C. Platt, J. Reuther, and R. Thomale, Phys. Rev. B **89**, 020408 (2014).
[9] O. I. Motrunich, Phys. Rev. B **72**, 045105 (2005).
[10] B. K. Clark, D. A. Abanin, and S. L. Sondhi, Phys. Rev. Lett. **107**, 087204 (2011).
[11] Z. Y. Meng, T. C. Lang, S. Wessel, F. F. Assaad, and A. Muramatsu, Nature **464**, 847 (2010).
[12] S. Sorella, Y. Otsuka, and S. Yunoki, Sci. Rep. **2**, 992 (2012).
[13] F. F. Assaad and I. F. Herbut, Phys. Rev. X **3**, 031010 (2013).
[14] D. Ixert, F. F. Assaad, and K. P. Schmidt, Phys. Rev. B **90**, 195133 (2014).
[15] S. R. Hassan and D. Sénéchal, Phys. Rev. Lett. **110**, 096402 (2013).
[16] M. Laubach, J. Reuther, R. Thomale, and S. Rachel, Phys. Rev. B **90**, 165136 (2014).
[17] A. A. Abrikosov and S. D. Beneslavskii, JETP **32**, 699 (1971).
[18] I. F. Herbut, Phys. Rev. Lett. **97**, 146401 (2006).
[19] L. Capriotti, A. E. Trumper, and S. Sorella, Phys. Rev. Lett. **82**, 3899 (1999).
[20] G. Khaliullin, Prog. Theor. Phys. Suppl. **160**, 155 (2005).
[21] G. Jackeli and G. Khaliullin, Phys. Rev. Lett. **102**, 017205 (2009).
[22] J. Reuther, R. Thomale, and S. Rachel, Phys. Rev. B **86**, 155127 (2012).
[23] I. Kimchi and A. Vishwanath, Phys. Rev. B **89**, 014414 (2014).
[24] D. Jaksch and P. Zoller, New. J. Phys. **5**, 56 (2003).
[25] J. Dalibard, F. Gerbier, G. Juzeliūnas, and P. Öhberg, Rev. Mod. Phys. **83**, 1523 (2011).
[26] N. R. Cooper, Phys. Rev. Lett. **106**, 175301 (2011).
[27] J. Struck, C. Ölschläger, M. Weinberg, P. Hauke, J. Simonet, A. Eckardt, M. Lewenstein, K. Sengstock, and P. Windpassinger, Phys. Rev. Lett. **108**, 225304 (2012).
[28] Y. Zhou and X.-G. Wen, cond-mat/0210662.
[29] T. Dey, A. V. Mahajan, P. Khuntia, M. Baenitz, B. Koteswararao, and F. C. Chou, Phys. Rev. B **86**, 140405 (2012).
[30] M. Becker, M. Herrmanns, B. Bauer, M. Garst, and S. Trebst, arXiv:1409.6972.
[31] K. Li, S.-L. Yu, and J.-X. Li, arXiv:1409.7820.
[32] I. Rousochatzakis, U. K. Rössler, J. van den Brink, and M. Daghofer, arXiv:1209.5895.
[33] M. Potthoff, Eur. Phys. J. B **36**, 335 (2003).
[34] M. Potthoff, Eur. Phys. J. B **32**, 429 (2003).
[35] P. Sahebsara and D. Sénéchal, Phys. Rev. Lett. **100**, 136402 (2008).
[36] A. H. MacDonald, S. M. Girvin, and D. Yoshioka, Phys. Rev. B **37**, 9753 (1988).
[37] R. Mishmash, J. Garrison, S. Bieri, and C. Xu, Phys. Rev. Lett. **111**, 157203 (2013).
[38] K. Ken and T. Momoi, Z. Phys. B **103**, 485 (1997).
[39] O. I. Motrunich, Phys. Rev. B **73**, 155115 (2006).
[40] H.-Y. Yang, A. M. Läuchli, F. Mila, and K. P. Schmidt, Phys. Rev. Lett. **105**, 267204 (2010).
[41] P. W. Anderson, Mater. Res. Bull. **8**, 153 (1973).
[42] D. S. Rokhsar and S. A. Kivelson, Phys. Rev. Lett. **61**, 2376 (1988).
[43] R. Moessner and S. L. Sondhi, Phys. Rev. Lett. **86**, 1881 (2001).
[44] F. Mila, F. Vernay, A. Ralko, F. Becca, P. Fazekas, and K. Penc, J. Phys.: Cond. Matt. **19**, 145201 (2007).
[45] F. Vernay, A. Ralko, F. Becca, and F. Mila, Phys. Rev. B **74**, 054402 (2006).
[46] T. Kashima and M. Imada, J. Phys. Soc. Jpn. **70**, 3052 (2001).